Utrecht University

Faculty of Sciences
Institute for Subatomic Physics

Bachelor Thesis

Flow analysis with Gapped Q-Cumulants

Author:
Wouter Varenkamp

Supervisors:
Prof. Dr. Raimond Snellings
Redmer Bertens MSc

January 14, 2015

Contents

Abstract

Anisotropic flow is an important observable in the study of the Quark-Gluon Plasma that is expected to be formed in heavy-ion collisions. Non-flow contributions caused by particle decay, jets and track splitting can bias flow measurements. This thesis describes the addition of an η-gap to the existing Q-Cumulants method to suppress non-flow. This so-called Gapped Q-Cumulants method is tested with Monte Carlo simulations and shown to be succesful in suppressing the non-flow contributions.

1 Introduction

ALICE (A Large Ion Collider Experiment) is one of the detectors at the Large Hadron Collider at CERN. It is primarily designed to study heavy-ion collisions with a centre of mass energy of 2.76 TeV. These collisions reproduce the extreme temperatures and densities that are expected to have existed in the first microseconds after the Big Bang [1]. In this hot and dense state, quarks and gluons are no longer bound into hadrons, but become deconfined and form the so-called Quark Gluon Plasma (QGP). The phase transition of hadronic matter to this deconfined state and the properties of the Quark Gluon Plasma are key issues for the ALICE physics program.

Anisotropic flow is an important observable in the experimental study of the QGP. When ions collide without forming the QGP, the resulting particles will distribute evenly in all directions (see Fig.1 left). When, however, a QGP is formed, the deconfined quarks will interact. If the system of quarks and gluons is large enough to reach a thermal equilibrium, a pressure gradient with respect to the surrounding vacuum is formed (see Fig.1 right). The assymetries in a non-central collision cause the pressure gradient and therefore the collective expansion to be anisotropic, this is called *anisotropic flow*. The anisotropic flow causes the energy and therefore the number of particles and momentum measured to depend on the azimuthal angle.

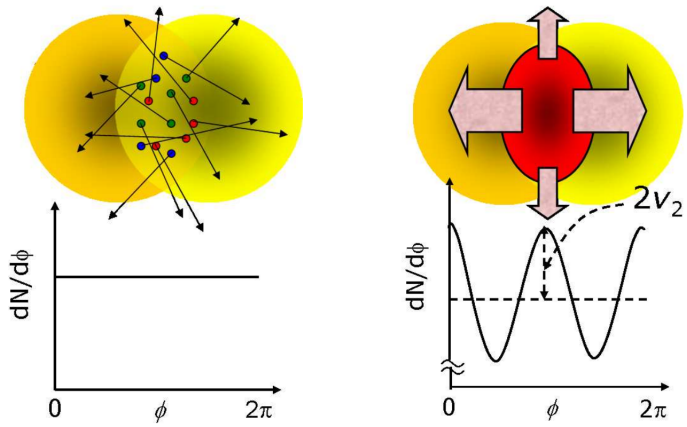

Figure 1: Schematic of two overlapping nuclei in the transverse to the beam direction, with particle density as a function of azimuthal angle. Left) Ion collision without the creation of a QGP, resulting in evenly distributed particles. Right) Ion collision with a QGP, resulting in an anisotropic particle distribution.

As the resulting particles and momentum are measured in a cylindrical detector, the azimuthal anisotropy is periodic and can be described by a Fourier series. The second coefficient of this series is called *elliptic flow*. The elliptic

flow is influenced by the pressure gradient and therefore provides information on the equation of state of the QGP.

One of the methods used to measure the elliptic flow is called 'Q-Cumulants', which uses 2- (or higher order) particle correlations. These 2-particle correlations are sensitive to the global anisotropic expansion, but also to local (short range) correlations, such as particle decay, track splitting and jets. These short range correlations are generally called 'non-flow' and will result in an overestimation of the elliptic flow. This paper introduces an η-gap in particle selection to improve the measurements by reducing the non-flow contibution. This so-called 'Gapped Q-Cumulants' method is added to the AliROOT FlowPackage and tested using Monte Carlo events.

Section 2 will discuss the concepts of (elliptic) flow and the QGP in more detail and introduces the concept of non-flow in 2-particle correlation measurements. Systems of the ALICE detector that are relevant to this research are described in section 3. Section 4 gives a detailed overview of the Gapped Q-Cumulants method. The Gapped-Q Cumulants results in the Monte Carlo simulations are discussed in chapter 5.

2 Theory

In Quantum Field Theory, Quantum Chromodynamics (QCD) is the theory which describes the strong interaction, a fundamental force describing the interactions between quarks and gluons. These are the building blocks of hadrons such as the proton, neutron and pion. One of the fundamental questions in QCD is what the properties of matter are at extreme densities and temperatures, where the quarks and gluons are in a deconfined state. This state is known as the Quark Gluon Plasma (QGP).

Heavy-ion collisions created at CERN are used to study the QGP. Figure 2 shows a time-space diagram of such a collision. At the origin, two heavy nuclei, A and B, collide. As shown, the system that is created will go through a variety of states. In the pre-equilibrium state, the nucleons inside the nuclei collide, freeing quarks and gluons. If the system is large and dense enough, a QGP phase can be formed where these quarks and gluons are deconfined and are in a local thermal equilibrium. The created QGP will expand and hadronize, creating particles that are measured in the ALICE detector. The collective expansion is called *flow*.

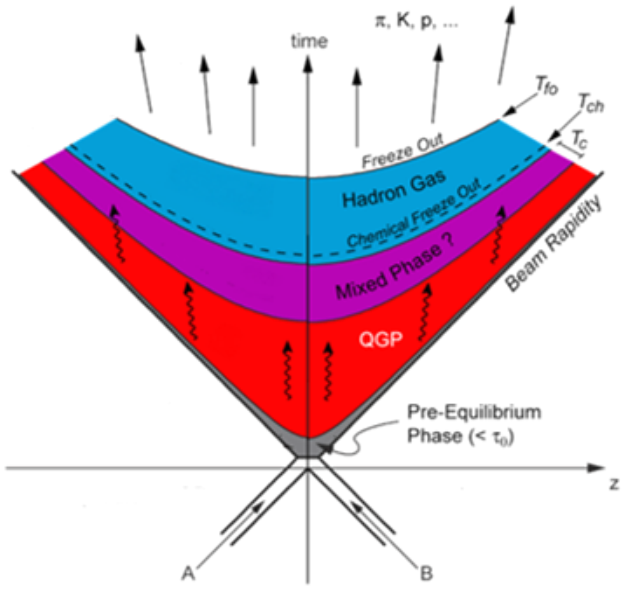

Figure 2: The system first forms a QGP and then partially hadronizes forming a Mixed Phase (consisting of hadrons and QGP). After the Chemical Freeze Out the system is fully hadronized, but the hadrons still interact. After the Freeze Out the final state is reached, which we measure in the detector.

In a QGP, the quarks and gluons are deconfined and interact, creating a pressure with respect to the surrounding vacuum. Generally, collisions are not head-on, creating an assymetric interaction volume (see Fig.3). Together this results in an anisotropic pressure gradient, causing the collective expansion (flow) to be anisotropic. This is called *anisotropic flow*.

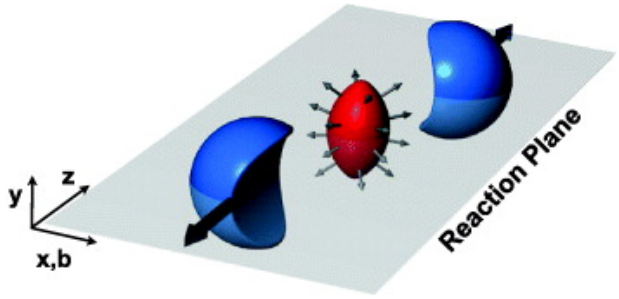

Figure 3: A non-central collision results in an assymetric interaction volume, which forms the QGP and creates an anisotropic pressure gradient. This results in an energy anisotropy and therefore the produced particles and momentum depend on the azimuthal angle.

The anisotropic flow leads to a periodic fluctuation in particle (energy) density, which can be experimentally quantified by a Fourier series:

$$\frac{dN}{d\varphi} = \frac{1}{2\pi}\left[1 + \sum_{n=1}^{\infty} 2v_n \cos(n(\varphi - \Psi_R))\right] \tag{1}$$

where N is the number of particles, φ is the particle's azimuthal angle, and Ψ_R the reaction plane angle (see Fig.4). The Fourier cofficients are given by:

$$v_n = \langle \cos[n(\varphi - \Psi_R)] \rangle \tag{2}$$

The angular brackets indicate an average over all particles in all events. The first coefficient v_1 is called directed flow, and the v_2 coefficient is called elliptic flow. This thesis will focus on measurements of v_2. The analysis code that is developed however can also be used to measure different harmonics.

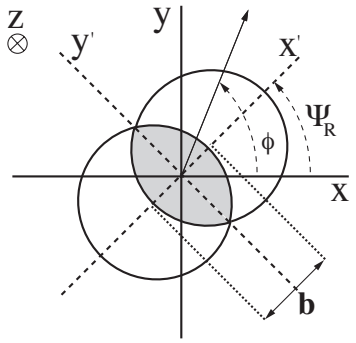

Figure 4: Schematic of the collision geometry in the transverse to the beam direction, with ϕ the azimuthal angle and Ψ_R the reaction plane angle.

Non-Flow

Using particle correlations, measurements of v_2 are sensitive to non-flow contributions. Particle decay, jets (narrow cones of hadrons produced by hadronization of a quark or gluon) and track splitting (the detector measures one track as two seperate tracks) result in particle correlations that are not caused by the flow of the QGP. This non-flow contribution causes an overestimation of the v_2 value. Figure 5 explains these non-flow correlations. The arrows that are drawn represent a projection in the transverse plane of momentum-vectors of particles that are created in a heavy-ion collision. In Fig. 5a we see a schematic representation of a system where there is a global correlation amongst all particles, the anisotropic flow, but no short range correlations. In this case the measured v_2 will correctly represent the anisotropic flow itself. In figure 5b we see no anisotropic flow, and a measurement will correctly result in the v_2 to be zero. However, as shown in figure 5c (with no anisotropic flow), the short range 2-particle correlations will contribute to the v_2 measurement and the measured v_2 will be greater than zero, even though there is no global correlation.

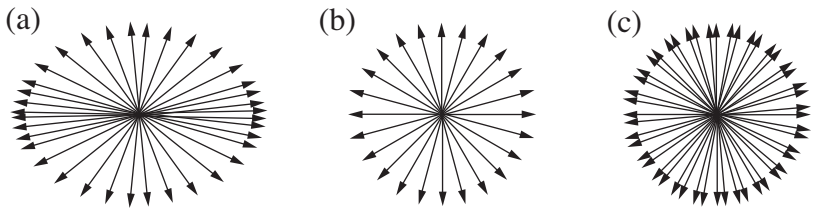

Figure 5: a) 'Real' $V_2 > 0$, V_2 from two-particle correlation > 0. b) 'Real' $V_2 = 0$, V_2 from two-particle correlation $= 0$. c) 'Real' $V_2 = 0$, V_2 from two-particle correlation > 0

The non-flow needs to be suppressed in the measurements to get the best v_2 estimates. The Gapped Q-cumulants method is specifically designed for this purpose. Non-flow correlations are short range, so when we only measure the correlation between particles that are separated in a longer range, we can reduce non-flow. This is realised by using an η-gap in particle selection. η is the psuedorapidity (see Fig.6), defined as

$$\eta = -\log\left(\tan\frac{\theta}{2}\right) \tag{3}$$

where θ is the angle between the particles momentum and the beam direction. It describes the particles direction relative to the beam axis.

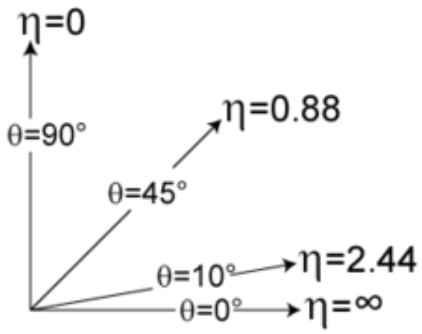

Figure 6: Psuedorapidity. The beam axis lies along $\eta = -\infty$ to ∞, which is schematically shown in Fig. 7

3 The ALICE detector

The results for the Gapped Q-Cumulants method found in this thesis are based on simulations, but the code that was developed for this study is compatible with data from the ALICE detector. The detector and the two most relevant components will be described in this section. These sub-systems are the ITS and TPC, which are the tracking systems of ALICE. The simulations that are used in this thesis mimick data coming from these two systems.

3.1 Introduction

ALICE is one of the seven detectors at CERN's Large Hadron Collider. The detector, shown in Figure 7, measures 16 x 16 x 26 m and weighs about 10.000 tonnes. It is designed to address the physics of strongly interacting matter and the quark-gluon plasma at extreme values of energy density and temperature in nucleus-nucleus collisions. It will allow for a comprehensive study of hadrons, electrons, muons, and photons produced in the collision of heavy nuclei (Pb-Pb) [2].

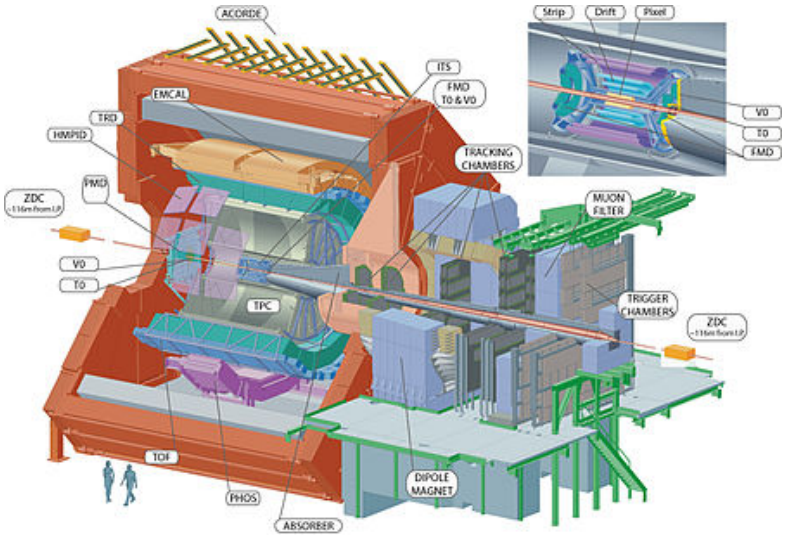

Figure 7: The ALICE detector

3.2 ITS

The Inner Tracking System (ITS) consists of six cilindrycal layers of silicon detectors (see Fig.8). The layers are grouped in three sets of two layers, forming three distinct detectors. The innermost are composed of Silicon Pixel Detector (SPD), the middle layers are Silicon Drift Detector (SDD) and the outermost are based on Silicon Strip Detector (SSD) [2]. The ITS is the closest detector

to the interaction point and the beam pipe. The beam pipe has a 6 cm radius, which is the physical boundary for the ITS inner radius. The outer radius is bound by the TPC detector.

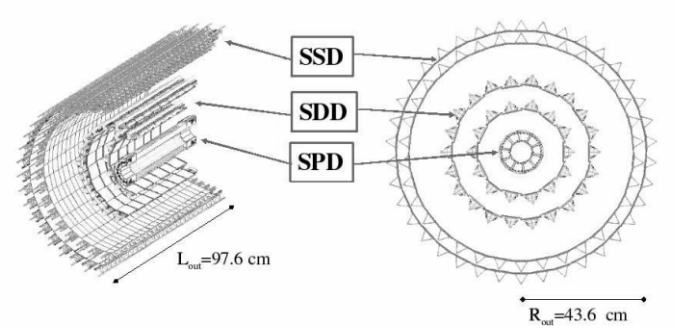

Figure 8: The ITS detector layout

The ITS is being used for primary vertex reconstruction and for the reconstruction of particle tracks. Transverse momentum is covered for $0.1 < p_t < 3$ GeV/c and the psuedorapitidy range is $|\eta| = 0.9$.

3.3 TPC

The Time Projection Chamber (TPC) is one of the biggest and most important components of ALICE. It measures 5m in longitude and is cylindrically shaped, with an inner radius of 85 cm and an outer radius of 250 cm. It is filled with a mixture of gases which is being ionized by the particles crossing the detector. The freed electrons drift towards the sides of the detector where they are measured. These measurements are used to calculate the coordinates of the ionization and can reconstruct a particles track in the detector.

The TPC is capable of detecting particles in the transverse momentum range $0.1 < p_t < 100$ GeV/c.The pseudorapidity coverage is $|\eta| < 0.9$ if only the tracks with maximum radial track length are being considered. Due to geometrical reasons, a higher η angle results in a lower track resolution. The TPC is also used to estimate collision centrality, which is a measure of the size of the interaction volume in a collision. In percentages, a 100% centrality means no interaction at all and 0% centrality indicates a head-on collision. This measurement is based on multiplicity, which is the number of particles observed in a detector after an event.

To summarize, a particle leaves a track in the detector which is used for analysis. The tracks are reconstructed using both TPC and ITS signals, and identified by using the TPC's signal.

4 Methods and implementation

4.1 Introduction

v_2 is defined as

$$v_n = \langle \cos[n(\varphi - \Psi_R)] \rangle \tag{4}$$

Experimentally however, the reaction plane angle Ψ_R is not available, so Eq. 4 cannot be evaluated directly. To overcome this, many different flow analysis techniques have been developed. Generally, these flow measurement methods can be divided into two categories. One way of estimating the flow is by reconstructing the event plane, which is an experimental estimate of Ψ_R. This method will be discussed in section 4.2. Another way of measuring flow is by using particle correlations directly. One of the methods using this principle is called Q-Cumulants and is discussed in section 4.3. The method introduced in this thesis is an extension of the already exisiting Q-Cumulants method and will be discussed in section 4.4. Finally, in section 4.5, the AliROOT FlowPackage will be reviewed.

4.2 Event Plane Method

The Event Plane method uses the anisotropic flow itself to estimate the azimuthal angle of the reaction plane (needed in Eq.1). This can be done for each harmonic, n, of the Fourier series. The event flow vector Q_n is a 2d vector in the transverse plane [3]:

$$Q_{n,x} = \sum_i w_i \cos(n\varphi_i) \tag{5}$$

$$Q_{n,y} = \sum_i w_i \sin(n\varphi_i) \tag{6}$$

The sum is over all particles used in the event plane calculation, with w_i and ϕ_i the weight and azimuthal angle for each particle. p_T (transverse momentum) is a common choice as a weight. The event plane angle, Ψ_{EP}, is the experimental estimate of angle Ψ_n and is the azimuthal angle of Q_n:

$$\Psi_{EP} = \text{arctan2}(Q_{n,x}, Q_{n,y})/n \tag{7}$$

Which is used to calculate v_n^{obs}:

$$v_n^{obs}(p_T, y) = \langle \cos[n(\varphi_i - \Psi_n)] \rangle \tag{8}$$

The angular brackets denote an average over all particles in all events, with φ_i in a given momentum and rapidity (y) space bin. v_n^{obs} has to be corrected by an experimentally determined resolution to correct for the fact that the flow has been evaluated with respect to the estimated event plane Ψ_{EP}, instead of the true underlying symmetry plane Ψ_n.

4.3 Q-cumulants Method

The Q-Cumulants method does not use the reconstruction of the event plane, but uses multi-particle correlations to estimate v_n directly. The following equation shows how the differential (for example as a function of transverse momentum) flow is measured using 2-particle correlations:

$$\begin{aligned} v_2' &= \frac{\langle v_2' \cdot v_2 \rangle}{\sqrt{\langle v_2 \cdot v_2 \rangle}} \\ &= \frac{\langle\langle 2' \rangle\rangle}{\sqrt{\langle\langle 2 \rangle\rangle}} \\ &= \frac{\langle \cos(n(\varphi_{POI} - \Psi_R)) \cdot \cos(n(\Psi_R - \varphi_{RFP})) \rangle}{\sqrt{\langle \cos(n(\varphi_{RFP} - \Psi_R)) \cdot \cos(n(\Psi_R - \varphi_{RFP})) \rangle}} \\ &= \frac{\langle \cos(n(\varphi_{POI} - \varphi_{RFP})) \rangle}{\sqrt{\langle \cos(n(\varphi_{RFP} - \varphi_{RFP})) \rangle}} \end{aligned} \tag{9}$$

where v_2' is the measured anisotropic flow, φ_{POI} and φ_{RFP} are the azimuthal angles of POI's and RFP's (the definition is given in the next paragraph). The prime indicates differential flow. This result includes a non-flow contribution caused by particle correlations independent of the anisotropic flow.

The Q-Cumulants method is basically an efficient way of evaluating Eq. 9. As can be seen here, all particles that are used in the analysis are labeled as POI's (Particles Of Interest, the particles of which the differential v_2 will be reported) or RFP (Reference Flow Particle). This is needed because the flow analysis is done in two steps. First the reference flow is estimated using only the RFP's. (The denominator of Eq. 9). Then the differential flow of POI's is estimated with respect to this reference flow. (The enumerator of Eq. 9).

By estimating the flow of POI's with respect to the reference flow, one can get a significant 2-particle correlation even when the number of POI's is small. This is because, as long as the RFP selection is large, a large number of particles will be used in the correlation term in the enumerator of Eq.9

The reference flow (denominator of Eq.9) is on an event-by-event basis as: [1]

$$\langle 2 \rangle \equiv \langle e^{in(\varphi_1 - \varphi_2)} \rangle = \frac{1}{P_{M,2}} \sum_{i,j}{}' e^{in(\varphi_1 - \varphi_2)} \tag{10}$$

where $P_{n,m} = n!/(n-m)!$ and the prime in the sum means that all indices must be taken differently. φ_1 and φ_2 are the azimuthal angles of particles from the RFP selection and M is the total number of RFP's.

[1] The Q-Cumulants have been studied and described in detail in [4]. The derivation of measuring v_n using 2-particle correlations in Q-Cumulants is reproduced here.

We average this correlation over all events:

$$\langle\langle 2\rangle\rangle = \langle\langle e^{in(\varphi_1-\varphi_2)}\rangle\rangle = \frac{\sum_{events}(W_{\langle 2\rangle})_i\langle 2\rangle_i}{\sum_{events}(W_{\langle 2\rangle})_i} \tag{11}$$

Where $W_{\langle 2\rangle} = M(M-1)$, which is introduced to give higher multiplicity events a bigger weight in the average. A higher mulitiplicity results in a stronger statistical significance of the correlation, which means more reliable results.

The correlation of the POI's and RFP's (enumerator of Eq. 9) is defined event-by-event as:

$$\langle 2'\rangle \equiv \langle e^{in(\varphi_i-\varphi_j)}\rangle = \frac{1}{m_pM - m_q}\sum_{i=1}^{m_p}\sum_{j=1}^{M} e^{in(\varphi_i-\varphi_j)} \tag{12}$$

Where m_p is the total number of POI's and m_q the total number of particles labeled both as RFP and POI. M is again the total number of particles labeled as RFP.

Event averaging is performed in the same way as eq. 11:

$$\langle\langle 2'\rangle\rangle = \frac{\sum_{events}(w_{\langle 2'\rangle})_i\langle 2'\rangle_i}{\sum_{events}(w_{\langle 2'\rangle})} \tag{13}$$

Where $w_{\langle 2'\rangle} = m_pM - m_q$

We can now calculate the differential flow of POI's :

$$v_2' = \frac{\langle v_2' \cdot v_2\rangle}{\sqrt{\langle v_2 \cdot v_2\rangle}} = \frac{\langle\langle 2'\rangle\rangle}{\sqrt{\langle\langle 2\rangle\rangle}} \tag{14}$$

A step-by-step implementation of the equations that have just been presented is not practical, since the number of 2-particle correlations scales with $\approx M^2$. To avoid this we can use the Q_n vector. Where

$$Q_n = \sum_{i=1}^{M} e^{in\varphi_i} \tag{15}$$

With M the total number of particles. By using this Q_n vector the amount of calculations needed is reduced from $M(M-1)$ to M.

Using the Q_n vector we can calculate $\langle 2\rangle$:

$$\langle 2\rangle = \frac{|Q_n|^2 - M}{M(M-1)} \tag{16}$$

Which is averaged by Eq. 11. The $-M$ term is used to cancel out autocorrelation.

We now introduce

$$p_n \equiv \sum_{i=1}^{m_p} e^{in\varphi_i} \tag{17}$$

to calculate $\langle 2' \rangle$:

$$\langle 2' \rangle = \frac{p'_n Q^*_n - m_q}{m_p M - m_q} \tag{18}$$

4.3.1 Sensitivity to non-flow effects

Earlier ALICE studies have used Q-Cumulants analyses where the POI and RFP selection was taken from the entire η range (see Fig.9). As explained in section 2, these measurements are sensitive to non-flow effects, caused by short range particle correlations. The next section will introduce the Gapped Q-Cumulants method, which uses an η-gap in particle selection to suppress the non-flow effects.

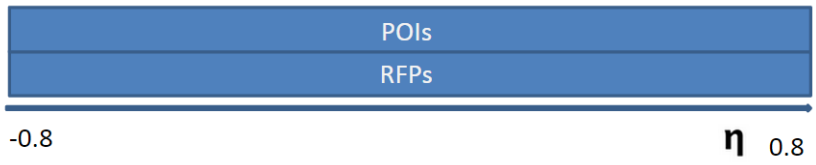

Figure 9: POI and RFP selection

4.4 Gapped Q-Cumulants

The Gapped Q-Cumulants method [**?**] is designed to suppress particle correlations that are not caused by the anisotropic expansion of the Quark Gluon Plasma. These correlations are due to particle decay, jets or track splitting. By adding an η-gap in the selection of POI's and RFP's (both chosen from a different η interval) the short range correlations will be taken of out the analysis (see Fig.10).

Figure 10: POI and RFP selection, with an η-gap

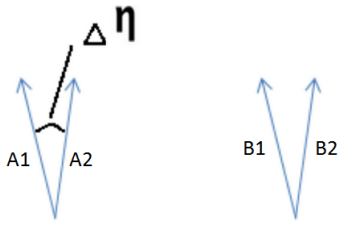

Figure 11: When the η-gap used in the analysis is larger than $\Delta\eta$ between two particles (for instance A1 and A2 in this figure), their short range correlation will not contribute to the flow measurement. Then only the global correlation (for instance between particle A1 and B2) will be used.

In the Gapped Q-Cumulants case, Eq. 9 is changed to:

$$\begin{aligned} v_2' &= \frac{\langle v_2' \cdot v_2 \rangle}{\sqrt{\langle v_2 \cdot v_2 \rangle}} \\ &= \frac{\langle\langle 2' \rangle\rangle}{\sqrt{\langle\langle 2 \rangle\rangle}} \\ &= \frac{\langle \cos(n(\varphi_{POI} - \Psi_R)) \cdot \cos(n(\Psi_R - \varphi_{RFPb})) \rangle}{\sqrt{\langle \cos(n(\varphi_{RFPa} - \Psi_R)) \cdot \cos(n(\Psi_R - \varphi_{RFPb})) \rangle}} \\ &= \frac{\langle \cos(n(\varphi_{POI} - \varphi_{RFPb})) \rangle}{\sqrt{\langle \cos(n(\varphi_{RFPa} - \varphi_{RFPb})) \rangle}} \end{aligned} \tag{19}$$

Due to the particle selection gap (the autocorrelation terms are no longer necessary) the equations from section 4.3 become:

$$\langle 2 \rangle = \frac{Q_n' \cdot Q_n^*}{M' M} \tag{20}$$

$$\langle 2' \rangle = \frac{p_n' \cdot Q_n^*}{m_p M} \tag{21}$$

Where Q_n' and Q_n are based on a seperate η interval. Q_n' for instance using the RFPa particles and Q_n the RFPb particles. The remaining part of the calculation of v_2' remains the same.

The η intervals have to be the same size in order for v_2 to cancel out of Eq. 19. A downside to the use of this gap is the loss of useable data.

4.5 AliROOT & Flow Package

AliROOT is a C++ data analysis framework designed for the ALICE detector. It contains a so called *FlowPackage* where several methods for flow analysis can be found. The Gapped Q-Cumulants code has been added to the FlowPackage and is ready to be used on data.

In short, the code that was developed is organized as follows: The data from the detector (or simulation) is saved per event and thus held in an event file, which is the starting point in every flow analysis.

The first step in the analysis is selecting events for physics analysis (see Fig.12). Event selection can for instance be based on centrality to show differences in results per centrality bin.

After this the POI and RFP selection is done. Generally, the RFP selection will contain all charged particles, whereas the POI selection depends on the type of research that is carried out. Selection also includes selecting on kinematic criteria, such as p_T, φ and η. The POI choice determines the particle of which the differential flow is measured.

The left over particle data is then passed on to one or more analysis methods as a *Flowevent*. One of these methods is the Gapped Q-Cumulants method discussed in this thesis. Running the selected data through these methods results in an output file containing various histograms which hold the results of the analysis.

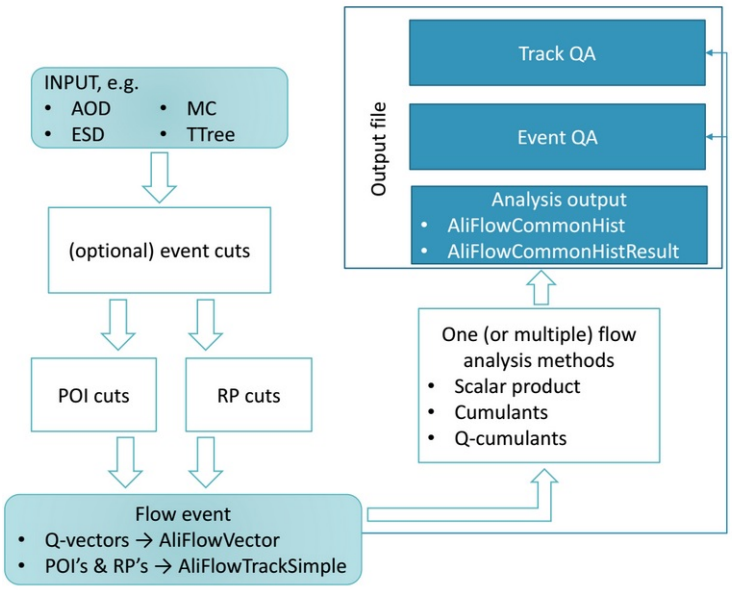

Figure 12: FlowPackage work order

The flow analysis methods are structured as shown in Fig. 13. In the function 'UserCreateOutputObjects' various histograms are created for storage. The next function, 'UserExec', contains the 'event loop', which runs the main analysis algorithm on one event at a time. UserExec stores the results from various calculations in the histograms created in the first step. Examples of these stored results are the values of $\langle 2 \rangle$ and $\langle 2' \rangle$ described in section 4.3. The final function 'Terminate' retrieves the stored values to calculate final results, such as v_2' and fills the histograms which hold the results of the analysis.

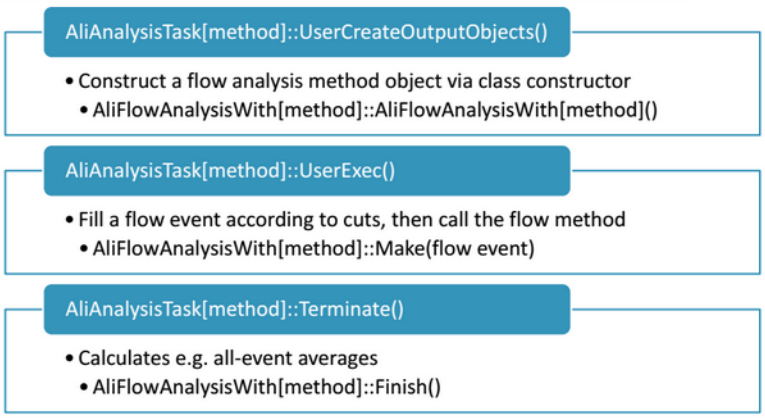

Figure 13: Code workflow. All AliROOT analysis tasks are structured using three functions. UserCreateOutputObjects initializes storage histograms, UserExec fills them with various calculation results from the event-loop and Terminate uses the stored results to calculate and store final results.

5 Results

The Gapped Q-Cumulants method is tested on simulated data. This section will start with a discussion of the 'On-The-Fly' simulations used. In section 5.2 the AliROOT code for the method will be reviewed for consistency and in section 5.3 the results for suppressing non-flow will be discussed. Section 5.4 describes an extension of the Gapped Q-Cumulants method which allows it to be used on detectors which have a non-uniform acceptance (i.e. are not evenly efficient in detecting particles in all azimuthal directions).

5.1 On-The-Fly

The Gapped Q-cumulants method will be tested using Monte Carlo events. These so-called 'On-The-Fly' simulations have a known v_2 input to compare with the results. The On-The-Fly simulation has a variety of parameters that can be chosen depending on the research interest, such as number of events and event multiplicity. Simulations in this thesis are done with one million generated events, each with a mulitiplicity of one thousand. The number of generated events is then in the same range as the number of events registered by ALICE in 2010 in one centrality interval of 10 %. The multiplicity chosen matches a 40-50% collision centrality. In all simulations the POI's are chosen to be in the $0.2 < p_t < 4$ GeV/c range and the RFP's in the $0.2 < p_t < 10$ GeV/c range. The η-gaps used are mentioned with the results.

The model simulates events by drawing random particle tracks in φ and η, creating an isotropic distribution. The input v_2 is then used to generate anisotropic events by changing the azimuthal angle of all tracks.

For an isotropic event:

$$\frac{dN}{d\varphi_0} = \frac{1}{2\pi} \tag{22}$$

Azimuthal anisotropy is described by Eq. 1, where the angle of the reaction plane is in principle arbitrary:

$$\frac{dN}{d\varphi} = \frac{1}{2\pi}\left[1 + \sum_{n=1}^{\infty} 2v_n \cos(n(\varphi - \Psi_R))\right] \tag{23}$$

Taking the 2nd harmonic and combining the two equations one arrives at

$$\frac{dN}{d\varphi} = \frac{dN}{d\varphi_0}\frac{d\varphi_0}{d\varphi} = \frac{1}{2\pi}\frac{d\varphi_0}{d\varphi} \tag{24}$$

which after integration over $\int \ldots d\varphi$ on both sides can be re-written as

$$\varphi = \varphi_0 - v_2 \sin\left[2\left(\varphi - \Psi_R\right)\right] \tag{25}$$

Where φ is the new azimuthal angle of the particle and v_2 the input value. Input v_2 can be given as a function of p_T. Each track is assigned transverse momentum from the following distribution:

$$\frac{dN}{dp_T} \propto p_T \cdot \exp\left(-\frac{\sqrt{0.13957^2 + p_T^2}}{0.4}\right) \tag{26}$$

which is a Boltzmann distribution for pions, which generally comprise 80% of the particles produced in a collision and therefore give a good first order approximation of the p_T spectrum of an event.

5.1.1 Non-flow contributions in On-The-Fly

A for this thesis very important feature of the simulation is the ability to 'clone tracks', so that close range correlations can be simulated. After an On-The-Fly event is created, all tracks are copied. The amount of tracks, M, is thereby doubled to 2M, of which M pairs are correlated with $\Delta\eta = 0$ and about M·M pairs are not correlated in a special way. This is used to test the Gapped Q-Cumulants ability to surpress non-flow.
All simulations are done with a known input $v_2(p_T)$, for which $v_2(p_T) = 0.05 * p_T$ for $0 < p_T < 0.5$ and $v_2(p_T) = 0.05$ for $p_T > 0.5$, which is represented by a black line in all graphs. This is a rough approximation of the v_2 found in ALICE data.

5.2 Code consistency

The AliROOT code is tested without introducing non-flow, using a chosen v_2 represented by the black line in figure 14. It is seen that the measured values are consistent with the input value and conclude that the code works properly. Note that in the first bin the center of the data point should have been at 0.350. The increasing uncertainty is due to the lower amount of data in the higher p_t bins. Figure 15 shows the RFP and POI selection.

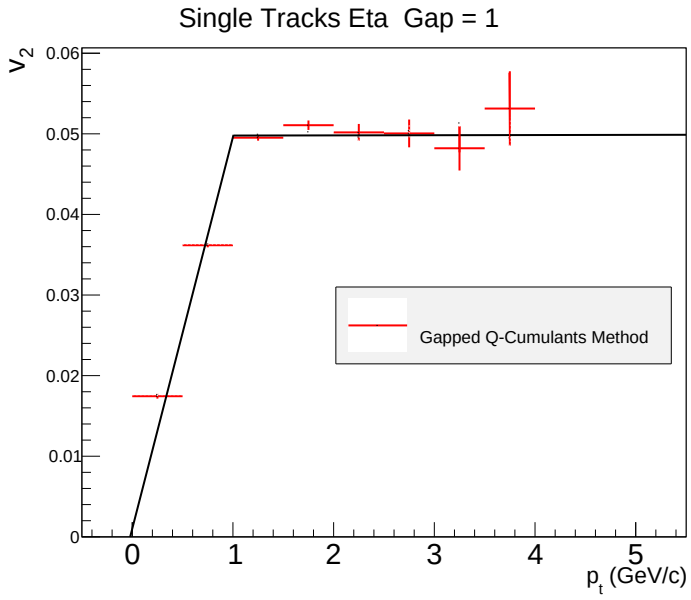

Figure 14: Code consistency check. No non-flow has been introduced. Black line: the input v_2 value. Red: measured v_2 by the GQC method.

Figure 15: POI and RFP selection used in Fig. 14

5.3 Elliptic flow measurements (v_2)

To test the sensitivity of the Gapped Q-Cumulants method to non-flow (short range) correlations, the analysis is performed on On-The-Fly events with cloned tracks. Each track in these events is copied, introducing M correlated pairs of tracks which are not separated in η, similar to figure 5c. Figures 16, 18 and 20 show simulations with the added non-flow. The v_2 value is estimated using two methods, the GQC method and the Scalar Product method (SPM). The SPM is comparable to the normal Q-Cumulants method and uses no η-gap in particle selection. The gap sizes used in the measurements are 0.6, 1 and 1.4, each shown in the figures below the results (Fig.17,19,21).

As expected, the Scalar Product method failes to reproduce the input v_2 in all three figures (Fig.16,18,20). It can be clearly seen that GQC method results in a better fit to the input flow. The bigger gap sizes show larger uncertainties as they use a smaller amount of data. There are no further resulting differences in the gap sizes used. This is due to the way of simulating non-flow. When using cloned tracks, even the smallest gap will separate all short range correlations. The differences shown in Figures 16,18 and 20 are only statistical.

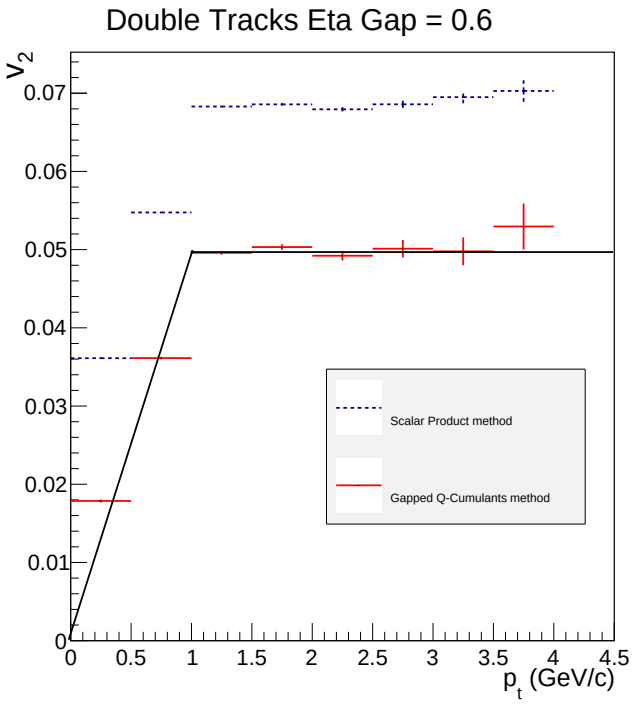

Figure 16: Sensitivity to non-flow of 2-particle correlation v_2 measurements. Non-flow introduced by cloning tracks. η-gap=0.6. Red: Gapped Q-Cumulants method. Blue: Scalar Product method. Black: input v_2. The Gapped Q-Cumulants method is able to reproduce the input v_2 even in the presence of short range correlations.

Figure 17: POI and RFP selection used in Fig. 16

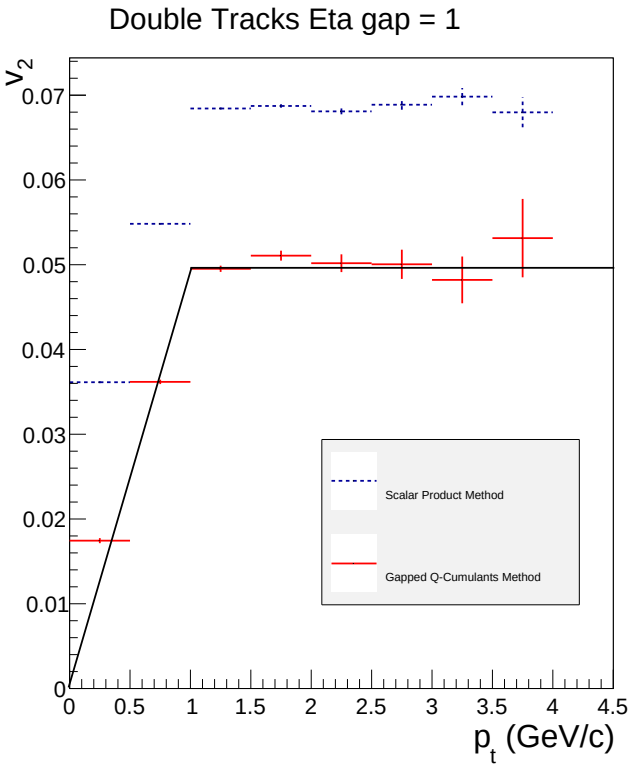

Figure 18: Sensitivity to non-flow of 2-particle correlation v_2 measurements. Non-flow introduced by cloning tracks. η-gap=1. Red: Gapped Q-Cumulants method. Blue: Scalar Product method. Black: input v_2. The Gapped Q-Cumulants method is able to reproduce the input v_2 even in the presence of short range correlations.

Figure 19: POI and RFP selection used in Fig. 18

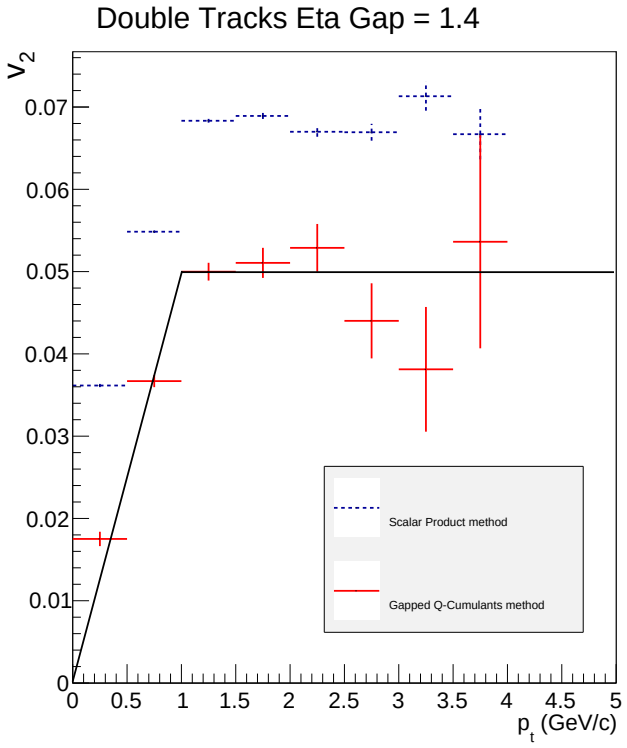

Figure 20: Sensitivity to non-flow of 2-particle correlation v_2 measurements. Non-flow introduced by cloning tracks. η-gap=1.4. Red: Gapped Q-Cumulants method. Blue: Scalar Product method. Black: input v_2. The Gapped Q-Cumulants method is able to reproduce the input v_2 even in the presence of short range correlations. Note that the larger gap sizes lead to increased statistical uncertainties.

Figure 21: POI and RFP selection used in Fig.20

5.4 Non-Uniform Acceptance

Detector deadzones (non-functioning parts of the detector) influence flow measurements when they are not corrected. A fully functioning detector has what is called 'Uniform Acceptance (UA)', whilst a detector with deadzone has 'Non-Uniform Acceptance'. Non-Uniform Acceptance increases the measured collective flow, because particles appear to be more correlated (see Fig.22). The On-The-Fly model can simulate a detector deadzone, by rejecting tracks based on their φ, η position. This section shows that the code succesfully corrects for detector deadzones.

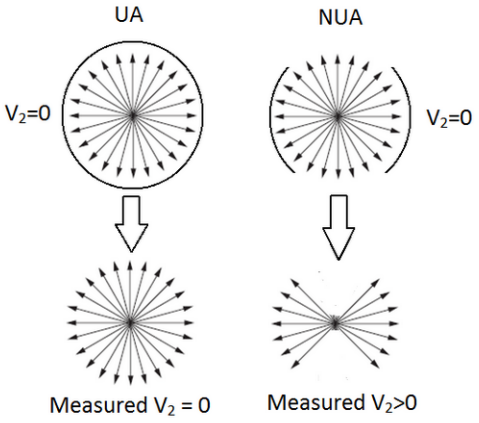

Figure 22: The top left of this figure shows an isotropic event being registered by a detector with full azimuthal coverage (depicted by the circle encapsulating the event). The full event is measured and no azimuthal anisotropy is measured ($v_2 = 0$). The right hand side shows the results of the same event, registered by a detector which has gaps in its coverage. The measured event is non-uniform, resulting in a measured $v_2 > 0$.

The corrections for a NUA detector have the following form (see Eq. 11 and Eq. 13):

$$\langle\langle 2\rangle\rangle \Rightarrow \langle\langle 2\rangle\rangle - \left\langle \frac{\mathrm{Re}(Q_n)}{m} \right\rangle^2 - \left\langle \frac{\mathrm{Im}(Q_n)}{m} \right\rangle^2 \tag{27}$$

$$\langle\langle 2'\rangle\rangle \Rightarrow \langle\langle 2'\rangle\rangle - \left\langle \frac{\mathrm{Re}(p_n)}{n} \right\rangle \left\langle \frac{\mathrm{Re}(Q_n)}{m} \right\rangle - \left\langle \frac{\mathrm{Im}(p_n)}{n} \right\rangle \left\langle \frac{\mathrm{Im}(Q_n)}{m} \right\rangle \tag{28}$$

Where n, m are the number of particles in each vector.

Whilst the UA calculations use standard error propagation, a different approach has been taken for the NUA corrected v_2 values, as the expressions resulting from the standard propagation are long and error-prone. The errors in the NUA values are calculated in the following way: the values of v_2 are calculated 1000 times using a random value from a gaussian distribution around each parameter. A distribution is built from the resulting v_2 values. The width of this distribution, obtained by fitting a Gaussian, is plotted as a 1 sigma (68 % confidence interval) on the differential v_2 results.

Figure 23 shows two simulation results for a detector *without* a deadzone. The blue line indicates the result for a analysis without a deadzone correction (UA), the red line does have a deadzone correction (NUA). As expected, no difference is found, as the simulation is runned without a deadzone. Uncertainties are larger in the NUA result because the corrected $\langle\langle 2\rangle\rangle$ and $\langle\langle 2'\rangle\rangle$ have additional terms which have an uncertainty as well, resulting in a larger overall uncertainty.

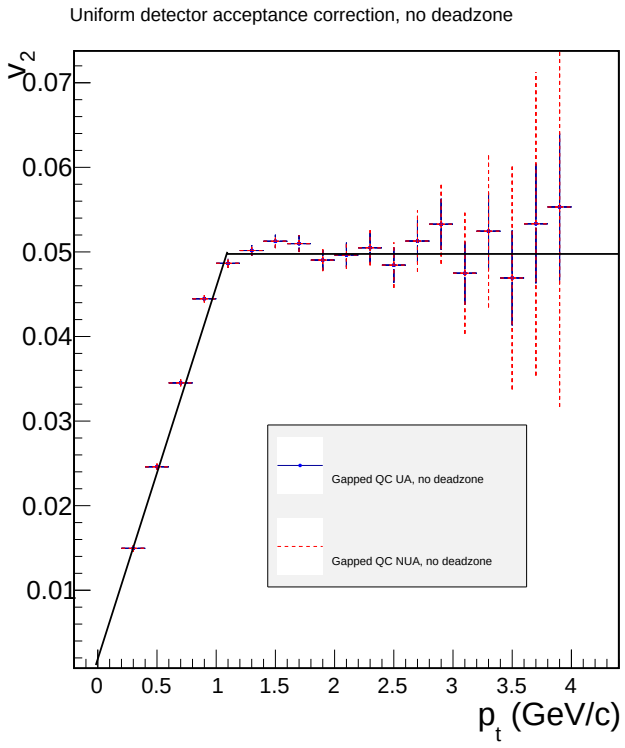

Figure 23: Blue: Uniform detector acceptance without simulated deadzone. Red: Non-Uniform detector acceptance without simulated deadzone. Black: Input v_2

Figure 24 shows what happens when a deadzone is simulated in the detector. The deadzone was simulated for $1 < \phi < 1.4$ and $-1 < \eta < 1$. The analysis is done for both UA (blue line) as with a NUA correction (red line). An uncorrected detector deadzone results in more particle correlation and therefore results in a higher v_2 result, as can be seen in the figure. The NUA correction succesfully corrects for the deadzone and matches the input v_2

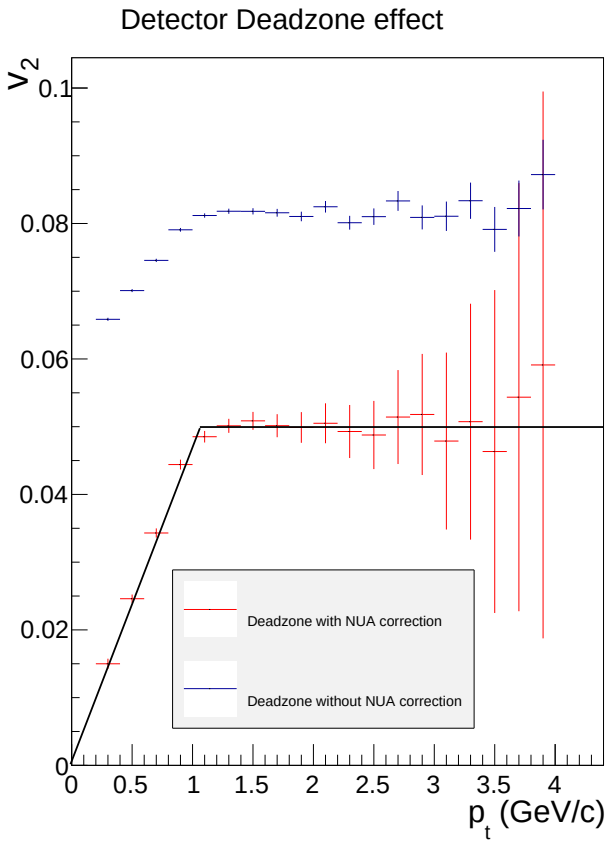

Figure 24: Comparison between v_2 measurements with and without NUA correction. Blue: Uniform detector acceptance with simulated deadzone. Red: Non-Uniform detector acceptance with simulated deadzone. Black: Input v_2

Figure 25 shows matching results for a detector with a deadzone compared to a detector without a deadzone. In both the blue (without deadzone) and red (with deadzone) results the NUA correction was used, which does nothing when there is no deadzone. We see no significant differences and both match the input v_2. The NUA results have larger uncertainties, as the deadzone causes a loss of data to use in the measurement.

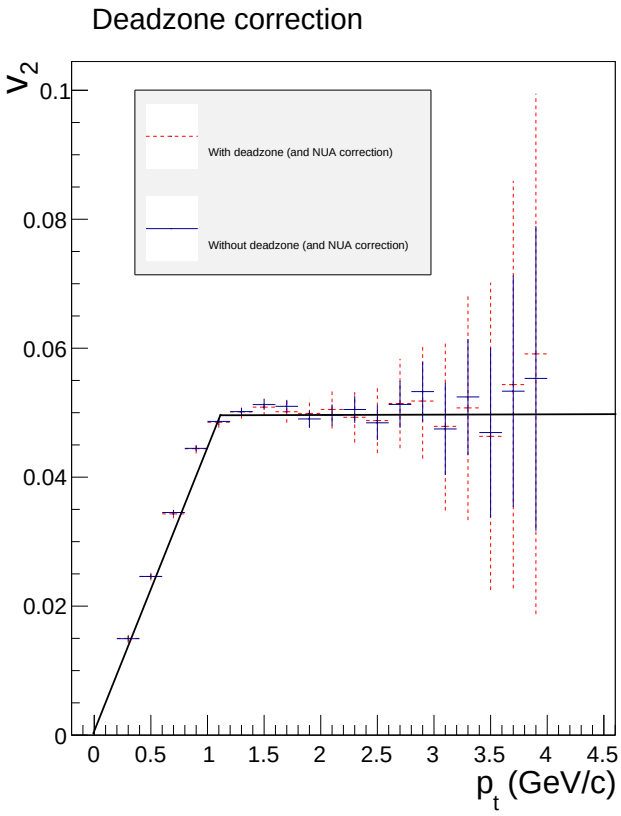

Figure 25: Blue: Non-Uniform detector acceptance without simulated deadzone. Red: Non-Uniform detector acceptance with simulated deadzone. Black: Input v_2

6 Conclusion & Outlook

In this thesis, a new 2-particle correlation method for measuring v_n, the Gapped Q-Cumulants, has been introduced an tested. The goal was to show the method's ability to surpress non-flow contributions in v_2 measurements. As shown in figures 16, 18 and 20, the method is succesful in On-The-Fly simulations using track doubling as non-flow. Where the Scalar Product method overestimates the v_2, the Gapped Q-Cumulants method surpresses the non-flow and correctly reproduces the input values.

The next step in research would be to use the new method on real data from the ALICE detector. It is expected that the measured v_2 from the Gapped Q-Cumulants method is closer to the actual v_2 value, due to the reduction of non-flow. A downside to this method is the loss of useable data. As the used particle tracks are selected from a smaller η interval, due to the gap (see Fig.10), fewer tracks are used in comparison to methods which do not deploy an η-gap in particle selection.

Additionally, the Gapped Q-Cumulants can be extended to 4- or higher particle correlations. However, a large number of tracks is necessary for this (imagine e.g. that one can create multiple 2-particle correlations from a collection of 3 tracks, but not one 4-particle correlation). Since the η-gap reduces the number of available tracks, it is not a-priori clear if higher-order particle correlations can be used in combination with η-gaps that are larger enough to suppress non-flow.

Lastly, more extensive model testing should be done by introducing more realistic types of non-flow to On-The-Fly events (e.g. introducing realistic decays and jets).

References

[1] Raimond Snellings, *Elliptic Flow: A Brief Review*. Utrecht University, 2011.

[2] Aamodt, K *et al* *The ALICE experiment at the CERN LHC*. Journal of Instrumentation 3, s08002, 2008.

[3] Poskanzer, A.M., Voloshin, S.A. *Methods for analyzing anisotropic flow in relativistic nuclear collisions*. Physicsal Review C, Volume 58, number 3, 1998

[4] Ante Bilandzic, Raimond Snellings, and Sergei Voloshin *Flow analysis with cumulants: direct calculations*. arXiv: 1010.0233v2, 2011.

[5] You Zhou, Sergei Voloshin *Private communication*.